GUST RESPONSE OF A TYPICAL SECTION VIA CFD AND ANALYTICAL SOLUTIONS

Berci M.[*], Mascetti S.[†], Incognito A.[†], Gaskell P.H.[*], Toropov V.V.[*]

[*]University of Leeds
Leeds, LS2 9JT, UK
M.Berci@leeds.ac.uk, P.H.Gaskell@leeds.ac.uk, V.V.Toropov@leeds.ac.uk

[†]XC Engineering
Cantu', 22063, Italy
Stefano.Mascetti@xceng.com, Alessandro.Incognito@xceng.com

Key words: Typical Section, Gust Response, Aeroelasticity, FSI, CFD, Airfoil

Abstract. *The gust response of a Typical Section is investigated in term of both high-fidelity Computational Fluid Dynamics (CFD) and low-fidelity analytical solutions of the aerodynamic flow around it, in order to assess the suitability of the two approaches in the preliminary design of a flexible wing. The aerodynamic forces acting over the oscillating airfoil are calculated using the high-fidelity commercial tool FLOW-3D and in term of the low-fidelity Theodorsen and Wagner theories formulated in a state-space form. A sinusoidal vertical gust acts as the aerodynamic perturbation to the static equilibrium of the aeroelastic system, the static and dynamic responses of which are provided for different airfoil shapes, Typical Section elastic properties, gust intensities and approaches. The effects of the physical differences between the two models are identified in the case of both attached and separated flow during the airfoil's aeroelastic response. For attached flow the low-fidelity gust response agrees well with the high-fidelity one, whereas for separated flow the low-fidelity model is unable to predict the strong oscillations of the Typical Section in dynamic stall conditions and suitable tuning of its response is needed.*

1 INTRODUCTION

In the context of aircraft preliminary design, reliable but computationally cheap tools are highly desirable for analysing aircraft integrity, stability, controllability and performance, due to the large number of design possibilities to be investigated. A multidisciplinary approach where aeroelasticity plays a key role[1] is nowadays required for this purpose and it is therefore interesting to verify the suitability of simplified, computationally cheap low-fidelity aeroelastic models relative to detailed, computationally expensive high-fidelity ones.

The gust response of a Typical Section[2] (see Figure 1) is considered, where the aerodynamic forces acting over the oscillating airfoil are calculated using both the high-fidelity CFD commercial tool FLOW-3D[3] and the low-fidelity Theodorsen[4] and Wagner[5] analytical theories. The section is an idealised representation of the cordwise rigid section of a spanwise flexible wing: it is located at about 80% of the wing span and consists of a rigid airfoil which can heave and pitch around the wing's elastic axis (EA), the elastic properties of which are represented by both a vertical spring k_h (for wing bending) and a torsional spring k_ϑ (for wing torsion); its mass m and principal second moment of inertia μ are concentrated at its centre of gravity (CG).
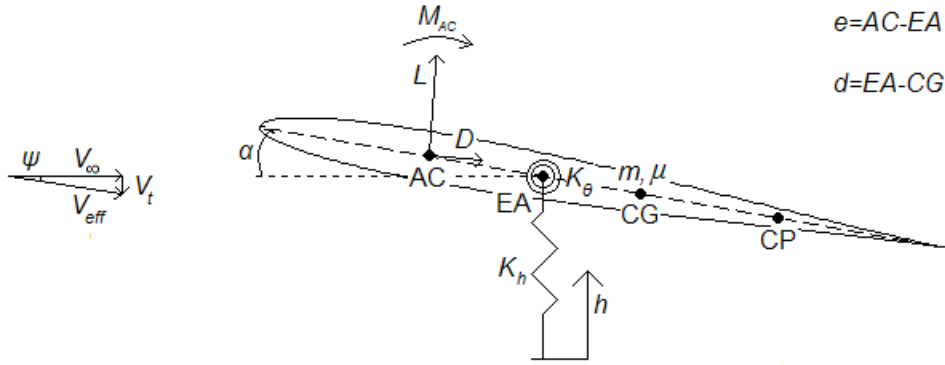

Figure 1: Typical Section sketch.

A vertical wind gust acts as the aerodynamic perturbation to the static equilibrium of the aeroelastic system and is introduced as a variation of the free-stream velocity either globally, the whole airfoil experiencing it at the same time, or locally, the airfoil penetrating it gradually. Both a light and a heavy gust have been applied in order to compare the dynamic response of the Typical Section as calculated by the low- and high-fidelity models for both attached flow with small airfoil displacements and separated flow with moderately large airfoil displacements.

2 AEROELASTIC MODELS

With $h = h(t)$ the vertical translation of the Typical Section and $\alpha = \alpha(t)$ its rotation about the wing elastic axis, by assuming the airfoil displacements to extend to moderately large values the following linear geometrical relationships hold

$$h_{AC} = h + e\alpha, \qquad h_{CG} = h - d\alpha, \qquad h_{CP} = h - \left(\frac{c}{2} - e\right)\alpha, \qquad \alpha = \alpha_r + \vartheta, \qquad (1)$$

where e and d are the distances of the aerodynamic centre and the centre of gravity from the elastic axis, respectively, α_r is the aircraft's rigid angle of attack in cruise configuration and $\vartheta = \vartheta(t)$ is the rotation of the elastic axis with respect to it.

By assuming the wing's structural damping to be neglegtable, the equations of motion (i.e., pitch and plunge equilibrium) of the Typical Section about the wing elastic axis are

$$m(\ddot{h} - d\ddot{\vartheta}) + k_h h = L - mg, \qquad \mu\ddot{\vartheta} - md(\ddot{h} - d\ddot{\vartheta}) + k_\vartheta \vartheta = M + dmg, \tag{2}$$

where $L = L(t)$ and $M = M(t)$ represent the total lift and aerodynamic moment resulting at the wing's elastic axis, which are given by

$$L = \int_0^c \Delta p\, dx, \qquad M = \int_0^c \Delta p\left[\left(\frac{c}{4} + e\right) - x\right] dx, \tag{3}$$

with $\Delta p = \Delta p(x,t) = \Delta \bar{p}(x) + \Delta \tilde{p}(x,t)$ the pressure distribution along the airfoil cord c, its leading edge being at $x = 0$ and trailing edge at $x = c$. Since the airfoil surface represents the boundary condition for the aerodynamic flow around it, the pressure distribution along the airfoil cord depends on its motion directly and a Fluid-Structure Interaction (FSI) problem is hence formulated.

The above system of two Ordinary Differential Equations (ODEs) can be suitably written in matrix form as

$$[M^s]\{\ddot{\chi}\} + [K^s]\{\chi\} = \{F^a\} + \{F^g\}, \qquad \{\chi\} = \begin{Bmatrix} h \\ \vartheta \end{Bmatrix}, \tag{4}$$

where the structural mass matrix $[M^s]$, structural stiffness matrix $[K^s]$, aerodynamic load vector $\{F^a\}$ (including the gust load) and gravity load vector $\{F^g\}$ are

$$[M^s] = \begin{bmatrix} m & -md \\ -md & \mu + md^2 \end{bmatrix}, \qquad [K^s] = \begin{bmatrix} k_h & 0 \\ 0 & k_\vartheta \end{bmatrix},$$
$$\{F^a\} = \begin{Bmatrix} L \\ M \end{Bmatrix}, \qquad \{F^g\} = \begin{Bmatrix} -mg \\ dmg \end{Bmatrix}, \tag{5}$$

and both the displacements vector $\{\chi\} = \{\chi(t)\}$ and the aerodynamic load vector $\{F^a\} = \{F^a(t)\}$ are generally composed of both a static contribution $\{\bar{\chi}\}$, $\{\bar{F}^a\}$ and a dynamic contribution $\{\tilde{\chi}\} = \{\tilde{\chi}(t)\}$, $\{\tilde{F}^a\} = \{\tilde{F}^a(t)\}$ as

$$\{\chi\} = \{\bar{\chi}\} + \{\tilde{\chi}\} = \begin{Bmatrix} \bar{h} \\ \bar{\vartheta} \end{Bmatrix} + \begin{Bmatrix} \tilde{h} \\ \tilde{\vartheta} \end{Bmatrix}, \qquad \{F^a\} = \{\bar{F}^a\} + \{\tilde{F}^a\} = \begin{Bmatrix} \bar{L} \\ \bar{M} \end{Bmatrix} + \begin{Bmatrix} \tilde{L} \\ \tilde{M} \end{Bmatrix}, \tag{6}$$

In cruise condition, the static equilibrium equations for the purely static contribution $\{\bar{\chi}\}$ of the airfoil displacements give

$$[K^s]\{\overline{\chi}\} = \{\overline{F}^a\} + \{F^g\}, \tag{7}$$

where the components $\overline{L}$ and $\overline{M}$ of the static aerodynamic load vector $\{\overline{F}^a\}$ are

$$\overline{L} = \int_0^c \Delta\overline{p}\, dx, \qquad \overline{M} = \int_0^c \Delta\overline{p}\left[\left(\frac{c}{4} + e\right) - x\right] dx, \tag{8}$$

with $\Delta\overline{p} = \Delta\overline{p}(x)$ being the purely steady pressure distribution along the airfoil cord.

During the gust response, the dynamic equilibrium equations for the purely dynamic contribution $\{\widetilde{\chi}\}$ of the airfoil displacements are

$$[M^s]\{\ddot{\widetilde{\chi}}\} + [K^s]\{\widetilde{\chi}\} = \{\widetilde{F}^a\}, \tag{9}$$

with initial conditions $\{\widetilde{\chi}(0)\} = \{0\}$ and $\{\dot{\widetilde{\chi}}(0)\} = \{0\}$, where the components $\widetilde{L} = \widetilde{L}(t)$ and $\widetilde{M} = \widetilde{M}(t)$ of the dynamic aerodynamic load vector $\{\widetilde{F}^a\}$ are given by

$$\widetilde{L} = \int_0^c \Delta\widetilde{p}\, dx, \qquad \widetilde{M} = \int_0^c \Delta\widetilde{p}\left[\left(\frac{c}{4} + e\right) - x\right] dx, \tag{10}$$

with $\Delta\widetilde{p} = \Delta\widetilde{p}(x,t)$ being the purely unsteady pressure distribution along the airfoil cord.

2.1 High-Fidelity Model

FlowScience's commercial tool FLOW-3D is a CFD based general purpose package for multi-scale and multi-physics problems and serves as the high-fidelity model in the present work. The pressure distribution along the airfoil cord is obtained by solving the incompressible Unsteady Reynolds Averaged Navier-Stokes (URANS) equations[6] on a fix and structured finite-difference computational grid in two dimensions, using a finite-volume numerical approximation[7] and employing the Re-Normalised Group (RGN) turbulence model[8].

The flow region is subdivided into a structured mesh of fixed rectangular cells, to each of which the local time-averaged values of all dependent variables are associated. All variables are located at the center of the cells except for the components of the flow velocity vector, which are located at the cells faces in a staggered grid arrangement. Multi-block meshing[3] is used to generate a variable spaced grid of nested blocks. All geometric features of the problem are embedded within the mesh by defining the Fractional Areas/Volumes (FAVOR) of the cells which are open to flow[3]. Control volumes are defined surrounding each dependent variable location in order to construct discrete numerical approximations of the governing equations. For each control volume, surface fluxes, surface stresses and body forces can be computed in terms of surrounding variable values; these quantities are then combined to form approximations for the conservation laws expressed by the equations of motion. Most terms in the fluid equations are evaluated explicitly using the current time-step values of the local variables (although various implicit options exist as well); nevertheless, pressure and velocity are coupled implicitly by using time-advanced pressure in the momentum equations and time-advanced velocity in the mass/continuity equation. This semi-

implicit formulation of the discrete equations allows for the efficient solution of low speed and incompressible flow problems. The basic numerical method used in FLOW-3D has a formal accuracy of first-order with respect to both time and space increments, however second-order accurate options are also available and have been used here. In any case, boundary conditions are at least first-order accurate in all circumstances; for instance, the FAVOR method is equivalent to a first-order interpolation of the boundary conditions in cells partially occupied by an obstacle. This particular approach becomes particularly useful when solving transient problems as in the present work. A standard RNG turbulence model has been adopted to describe the fluctuations of the unsteady flow, where two coupled transport equations are written for the turbulent kinetic energy k and dissipation ε. In addition, FLOW-3D employs the General Moving Obstacle (GMO) model and Springs and Ropes (SR) physics to model the structural features of the Typical Section. The former is able to solve the equations of motion for a rigid body with up to six degrees of freedom, by employing a fixed-mesh approach which guarantees a fast and robust physical model; the latter allows multi-body dynamics representation by linking several solid objects together via springs (vertical, horizontal or torsional) and ropes.

The static aerodynamic load in cruise conditions is calculated starting from the initial rigid position of the airfoil; the static aeroelastic response of the Typical Section is then obtained as the asymptotic value of its dynamic response to the aerodynamic load due to free-stream wind.

Once the static aeroelastic response of the Typical Section is reached, a vertical gust travelling towards the airfoil is introduced as a perturbation of the free-stream wind and the dynamic aeroelastic response of the Typical Section to the additional aerodynamic load due to the gust is then calculated.

Two detailed views of the multi-block mesh employed for the FSI simulations are shown in Figure 2. The external mesh is about $30\,c$ along-wind and $15\,c$ cross-wind.
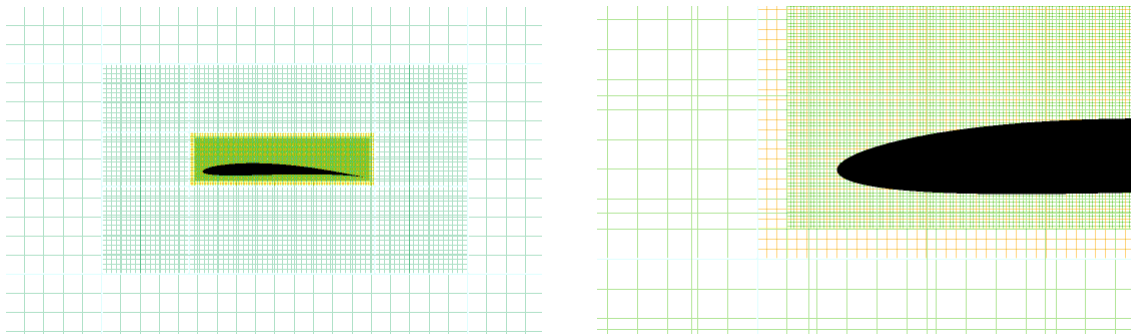

Figure 2: Typical multi-block CFD mesh: airfoil and leading edge close-up.

2.2 Low-Fidelity Model

Both Theodorsen's and Wagner's analytical theories serve as the low-fidelity model in the present work and are based on a two-dimensional, laminar, incompressible, inviscid and irrotational flow.

Linear thin airfoil theory[9] based on the complex kinetic potential for small flow perturbations is employed to estimate the aerodynamic load. The non-penetration boundary condition of the fluid flow over the oscillating airfoil is imposed at the airfoil Control Point (CP), located at the third quarter of its cord. The static lift $\overline{L}$ and aerodynamic moment $\overline{M}_{AC}$ of the airfoil are circulatory and applied at its Aerodynamic

Centre (AC), located at the first quarter of its cord, whereas both the dynamic lift $\tilde{L}$ and aerodynamic moment $\tilde{M}$ include additional circulatory and non-circulatory contributions applied at the control point and mid-cord, respectively. Both static drag $\overline{D}$ and dynamic drag $\tilde{D} = \tilde{D}(t)$ include a leading edge suction contribution[10] and are equal to zero, such that the total inviscid drag $D(t) = \overline{D} + \tilde{D}(t)$ is equal to zero too[11].

In cruise conditions, the static aerodynamic load on the airfoil results[2]

$$\overline{L} = \frac{1}{2}\rho_\infty V_\infty^2 SC_{\overline{L}/\alpha}\left(\alpha_r + \overline{\vartheta} - \alpha_0\right), \qquad \overline{M} = \frac{1}{2}\rho_\infty V_\infty^2 S\left[cC_{\overline{M}_{AC}} + eC_{\overline{L}/\alpha}\left(\alpha_r + \overline{\vartheta} - \alpha_0\right)\right], \quad (11)$$

where ρ_∞ is the air density, V_∞ the air speed and S the airfoil surface, whereas $C_{\overline{L}/\alpha}$ is the lift-curve slope coefficient and $C_{\overline{M}_{AC}}$ the aerodynamic moment coefficient of the airfoil, which can be obtained at its aerodynamic center by employing either the Prandtl-Glauert theory or the complex conformal theory for thin airfoils. The static aeroelastic equations of the Typical Section can then be written explicitly as

$$[K]\{\overline{\chi}\} = \left\{\overline{F}_r^a\right\} + \left\{F^g\right\}, \tag{12}$$

and their solution $\{\overline{\chi}\}$ calculated analytically; the aeroelastic stiffness matrix $[K]$ and the rigid aerodynamic load vector $\left\{\overline{F}_r^a\right\}$ are defined in Appendix A.

During the gust response of the Typical Section, a vertical component $\vec{V}_t$ of the free-stream velocity is generated by both the airfoil motion and the vertical gust; nevertheless, by considering small perturbations of the potential flow about the horizontal reference wind speed $\vec{V}_\infty$, the effective reference wind speed results $\vec{V}_{eff} = \vec{V}_\infty + \vec{V}_t \approx \vec{V}_\infty$. Based on this assumption, Theodorsen derived the purely dynamic aerodynamic load of the airfoil, which, by employing a suitable Pade' approximation of the complex Theodorsen's function[12] (which is defined in the reduced frequency domain), can be written in state-space form as

$$\tilde{L} = \frac{\pi}{4}\rho_\infty Sc\left\{V_\infty\dot{\tilde{\vartheta}} - \left[\ddot{\tilde{h}} - \left(\frac{c}{4}-e\right)\ddot{\tilde{\vartheta}}\right]\right\} + \frac{1}{4}\rho_\infty V_\infty^2 SC_{\overline{L}/\alpha}\left\{\tilde{\vartheta} - \frac{1}{V_\infty}\left[\dot{\tilde{h}} - \left(\frac{c}{2}-e\right)\dot{\tilde{\vartheta}} + \tilde{z}\right]\right\} + \tilde{L}^G,$$

$$\tilde{M} = -\frac{\pi}{4}\rho_\infty Sc\left\{\left(\frac{c^2}{32}\right)\ddot{\tilde{\vartheta}} + V_\infty\left(\frac{c}{2}-e\right)\dot{\tilde{\vartheta}} - \left(\frac{c}{4}-e\right)\left[\ddot{\tilde{h}} - \left(\frac{c}{4}-e\right)\ddot{\tilde{\vartheta}}\right]\right\} + \tag{13}$$

$$+ \frac{1}{4}\rho_\infty V_\infty^2 SeC_{\overline{L}/\alpha}\left\{\tilde{\vartheta} - \frac{1}{V_\infty}\left[\dot{\tilde{h}} - \left(\frac{c}{2}-e\right)\dot{\tilde{\vartheta}}\right] + \tilde{z}\right\} + \tilde{M}^G,$$

where $\tilde{L}^G = \tilde{L}^G(t)$ and $\tilde{M}^G = \tilde{M}^G(t)$ represent the additional aerodynamic load due to the gust, whereas $\tilde{z} = \tilde{z}(t)$ is an added aerodynamic state which evolves as

$$\left(\frac{c}{2V_\infty}\right)^2\ddot{\tilde{z}} + 0.552\left(\frac{c}{2V_\infty}\right)\dot{\tilde{z}} + 0.044\tilde{z} =$$

$$= 0.234\left(\frac{c}{2V_\infty}\right)\left\{\dot{\tilde{\vartheta}} - \frac{1}{V_\infty}\left[\ddot{\tilde{h}} - \left(\frac{c}{2}-e\right)\ddot{\tilde{\vartheta}}\right]\right\} + 0.044\left\{\tilde{\vartheta} - \frac{1}{V_\infty}\left[\dot{\tilde{h}} - \left(\frac{c}{2}-e\right)\dot{\tilde{\vartheta}}\right]\right\}, \tag{14}$$

with the static initial conditions $\tilde{z}(0) = 0$ and $\dot{\tilde{z}}(0) = 0$. The dynamic aeroelastic equations of the Typical Section can then be written explicitly as

$$[M^T]\{\ddot{\tilde{\xi}}\} + [C^T]\{\dot{\tilde{\xi}}\} + [K^T]\{\tilde{\xi}\} = \{\tilde{F}^G\}, \qquad \{\tilde{\xi}\} = \begin{Bmatrix} \tilde{h} \\ \tilde{\vartheta} \\ \tilde{z} \end{Bmatrix}, \qquad (15)$$

and their solution $\{\tilde{\xi}\}$ calculated analytically; the aeroelastic mass matrix $[M^T]$, damping matrix $[C^T]$, stiffness matrix $[K^T]$ and the gust aerodynamic load vector $\{\tilde{F}^G\}$ are defined in Appendix A.

By adopting an indicial approach with Duhamel integral convolution, Wagner derived an alternative formulation for the purely dynamic aerodynamic load of the airfoil, which, by a employing a suitable exponential approximation[13,14] of the Wagner's function (which represents the Fourier transform of the Theodorsen's function and is defined in the reduced time domain), can be written in state-space form as

$$\tilde{L} = \frac{\pi}{4}\rho_\infty Sc\left\{V_\infty\dot{\tilde{\vartheta}} - \left[\ddot{\tilde{h}} - \left(\frac{c}{4} - e\right)\ddot{\tilde{\vartheta}}\right]\right\} + \frac{1}{4}\rho_\infty V_\infty^2 SC_{\bar{L}/\alpha}\left\{\tilde{\vartheta} - \frac{1}{V_\infty}\left[\dot{\tilde{h}} - \left(\frac{c}{2} - e\right)\dot{\tilde{\vartheta}}\right]\right\} +$$

$$-\frac{1}{2}\rho_\infty V_\infty SC_{\bar{L}/\alpha}\left[0.108\left(\frac{2V_\infty}{c}\right)\dot{\tilde{w}} + 0.0068\left(\frac{2V_\infty}{c}\right)^2\tilde{w}\right] + \tilde{L}^G,$$

$$\tilde{M} = -\frac{\pi}{4}\rho_\infty Sc\left\{\left(\frac{c^2}{32}\right)\ddot{\tilde{\vartheta}} + V_\infty\left(\frac{c}{2} - e\right)\dot{\tilde{\vartheta}} - \left(\frac{c}{4} - e\right)\left[\ddot{\tilde{h}} - \left(\frac{c}{4} - e\right)\ddot{\tilde{\vartheta}}\right]\right\} + \qquad (16)$$

$$+\frac{1}{4}\rho_\infty V_\infty^2 SeC_{\bar{L}/\alpha}\left\{\tilde{\vartheta} - \frac{1}{V_\infty}\left[\dot{\tilde{h}} - \left(\frac{c}{2} - e\right)\dot{\tilde{\vartheta}}\right]\right\} +$$

$$-\frac{1}{2}\rho_\infty V_\infty SeC_{\bar{L}/\alpha}\left[0.108\left(\frac{2V_\infty}{c}\right)\dot{\tilde{w}} + 0.0068\left(\frac{2V_\infty}{c}\right)^2\tilde{w}\right] + \tilde{M}^G,$$

where $\tilde{w} = \tilde{w}(t)$ is an added aerodynamic state which evolves as

$$\ddot{\tilde{w}} + 0.3455\left(\frac{2V_\infty}{c}\right)\dot{\tilde{w}} + 0.136\left(\frac{2V_\infty}{c}\right)^2 w = \dot{\tilde{h}} - \left(\frac{c}{2} - e\right)\dot{\tilde{\vartheta}} - V_\infty\tilde{\vartheta}, \qquad (17)$$

with the static initial conditions $\tilde{w}(0) = 0$ and $\dot{\tilde{w}}(0) = 0$. The dynamic aeroelastic equations of the Typical Section can then be written explicitly as

$$[M^W]\{\ddot{\tilde{\zeta}}\} + [C^W]\{\dot{\tilde{\zeta}}\} + [K^W]\{\tilde{\zeta}\} = \{\tilde{F}^G\}, \qquad \{\tilde{\zeta}\} = \begin{Bmatrix} \tilde{h} \\ \tilde{\vartheta} \\ \tilde{w} \end{Bmatrix}, \qquad (18)$$

and their solution $\{\tilde{\zeta}\}$ calculated analytically; the aeroelastic mass matrix $[M^W]$, damping matrix $[C^W]$, stiffness matrix $[K^W]$ are defined in Appendix A.

The occurrence of a vertical gust $V_G = V_G(t)$ can be introduced as a variation of the free-stream velocity either globally or locally. In the sense of a "global" approach, the gust is experienced by the whole airfoil at the same time and can be modelled as an instantaneous variation of the vertical component of the effective reference wind speed (i.e., instantaneous angle of attack of the airfoil) by simply considering $\dot{\bar{h}}_{eff} = \dot{\bar{h}} - V_G$, modifying the evolution of the added aerodynamic states and generating the additional aerodynamic load

$$\widetilde{L}^G = \frac{\pi}{4}\rho_\infty Sc\dot{V}_G + \frac{1}{4}\rho_\infty V_\infty SC_{\overline{L}/\alpha}V_G,$$

$$\widetilde{M}^G = -\frac{\pi}{4}\rho_\infty Sc\left(\frac{c}{4} - e\right)\dot{V}_G + \frac{1}{4}\rho_\infty V_\infty SeC_{\overline{L}/\alpha}V_G.$$

(19)

In terms of a "local" approach, the airfoil gradually penetrates the gust travelling towards it and, still by adopting an indicial approach with Duhamel integral convolution, Kussner[15] derived its additional aerodynamic load, which, by employing a suitable exponential approximation[13,14] of the Kussner's function, can be written in state-space form as

$$\widetilde{L}^G = \frac{1}{2}\rho_\infty V_\infty SC_{\overline{L}/\alpha}\left[0.565\left(\frac{2V_\infty}{c}\right)\dot{\widetilde{g}} + 0.13\left(\frac{2V_\infty}{c}\right)^2\widetilde{g}\right],$$

$$\widetilde{M}^G = \frac{1}{2}\rho_\infty V_\infty SeC_{\overline{L}/\alpha}\left[0.565\left(\frac{2V_\infty}{c}\right)\dot{\widetilde{g}} + 0.13\left(\frac{2V_\infty}{c}\right)^2\widetilde{g}\right],$$

(20)

where $\widetilde{g} = \widetilde{g}(t)$ is a further added aerodynamic state which depends on the gust profile only (i.e., it is uncoupled from the airfoil motion) and evolves as

$$\ddot{\widetilde{g}} + 1.13\left(\frac{2V_\infty}{c}\right)\dot{\widetilde{g}} + 0.13\left(\frac{2V_\infty}{c}\right)^2\widetilde{g} = V_G,$$

(21)

with the static initial conditions $\widetilde{g}(0) = 0$ and $\dot{\widetilde{g}}(0) = 0$.

3 RESULTS

The Typical Section of a small aircraft of 550mm wing span, 100mm wing cord and 50mm fuselage width is considered. The aircraft wing is rectangular, has no wash-out, sweep and dihedral angle, its structural arrangement is uniformly made of balsa wood (density $\rho = 150$kg/m^3, Young's modulus $E = 1.3 \cdot 10^9$Pa, shear modulus $G = 6.2 \cdot 10^8$Pa) and consists of a single straight spar with rectangular section and ribs. The airfoil shape is given by the Karman-Trefftz conformal transformation[16] as

$$z = \frac{k_{KT}(c_{KT} - 1)}{\left(\dfrac{Z-1}{Z-c_{KT}}\right)^{k_{KT}} - 1}, \qquad k_{KT} = \frac{(360 - \alpha_T)}{180},$$

(22)

where $z = x + iy$ and $Z = X + iY$ are complex variables describing the airfoil shape (with a trailing edge angle $\alpha_T = 2\text{deg}$) and the unitary circle in the $x - y$ and $X - Y$ complex planes, respectively. As shown in Table 1, two different values for the complex constant c_{KT} have been chosen in order to generate two different airfoil shapes "A1" and "A2" with the same thickness distribution but different camber line. In particular, the maximum thickness of the airfoils is located at about 30% of their cord, where the wing spar is placed. Due to the small camber of the airfoils, their inertial properties are considered to be identical with their centre of gravity located at about 40% of their cord: for airfoils of width 30mm, their mass and principal second moment of inertia are estimated as $m = 2 \cdot 10^{-4}\text{kg}$ and $\mu = 10^{-7}\text{kg} \cdot \text{m}^2$. The cord $\hat{c}$ of the airfoils in the complex plane $x - y$ is defined as the maximum segment inscribable within the airfoils themselves, therefore their entire shape is rescaled in order to give the desired real cord c. The zero-lift direction being coincident with the horizontal axis of the $x - y$ complex plane, the zero-lift angle of attack α_0 of the airfoils is calculated as the angle between their cord and the x axis. The two Karman-Trefftz airfoils considered are shown in Fig. 3 and, by employing complex potential conformal theory[16], their static aerodynamic moment coefficient and lift-curve slope can be calculated as

$$C_{\bar{M}_{AC}} = -\frac{\pi}{3}\left(\frac{2}{\hat{c}^2}\right)\text{Im}\left(k_{KT}^2 (c_{KT} - 1)^2 + 3k_{KT}(c_{KT} - 1)(c_{KT} + 1) + 2(c_{KT}^2 + c_{KT} + 1)\right) +$$
$$+ \pi\left(\frac{4}{\hat{c}^2}\right)\text{Im}\left(\left(\frac{1}{2}k_{KT}\left[k_{KT}(c_{KT} - 1) + (c_{KT} + 1)\right]\right)^2\right), \qquad C_{\bar{L}/\alpha} = 2\pi\left(\frac{4}{\hat{c}}\right). \qquad (23)$$
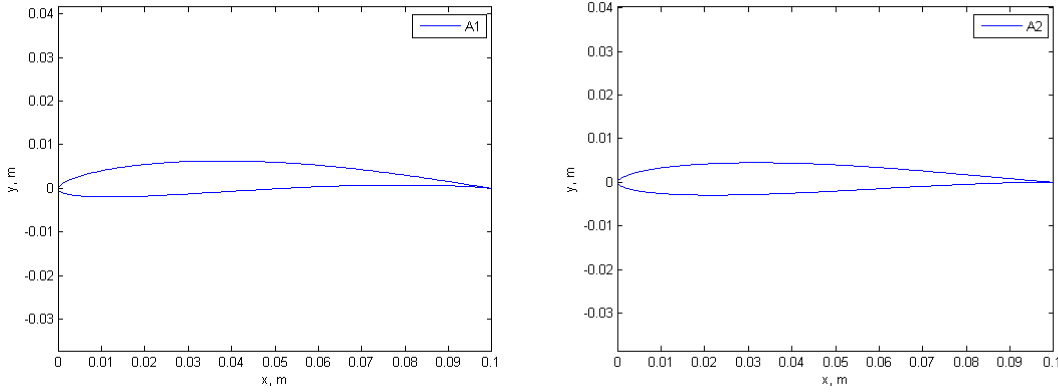

Figure 3: Karman-Trefftz airfoils.

Assuming the wing skin to play no structural role, the vertical and torsional springs of the Typical Section represent the wing spar flexibility only and their constants are calculated using the Principle of Virtual Work (PVW) and the Euler-Bernoulli beam approximation[17] as

$$k_h = \frac{3EI}{l^3}, \qquad k_\vartheta = \frac{GJ}{l}, \qquad (24)$$

where $l = 200\text{mm}$ is the spanwise location of the Typical Section, whereas I and J are the second moment of area and the torsion constant of the wing spar section about its

central horizontal axis, which are calculated employing the Saint-Venant torsion formulation[18] for a straight uniform bar of rectangular solid section as

$$I = \frac{h_s^3 w_s}{12}, \qquad J = \hat{a}\hat{b}^3 \left[\frac{1}{3} - 0.21 \frac{\hat{b}}{\hat{a}} \left(1 - \frac{\hat{b}^4}{12\hat{a}^4} \right) \right], \qquad (25)$$

with h_s =5mm the height and w_s the width of the wing spar cross-section, $\hat{a}$ and $\hat{b}$ being its larger and smaller dimension. The two values chosen for the wing spar width are shown in Table 1 and lead to two couples of values "S1" and "S2" for the linear springs constants.

	c_{KT}	α_0	$C_{\overline{L}/\alpha}$	$C_{\overline{M}_{AC}}$
A1	-0.89-0.11i	3.4deg	6.67	-0.09
A2	-0.90-0.04i	1.1deg	6.65	-0.03

	w_s	k_h	k_ϑ
S1	0.0084m	42.5N/m	0.68Nm/rad
S2	0.0051m	26.0N/m	0.29Nm/rad

Table 1: Typical Section parameters: airfoils and springs.

A sinusoidal vertical gust of one-second duration is considered as a perturbation of the aeroelastic system in cruise conditions

$$V_G = \frac{V_G}{2}(1 + \cos(\pi t)), \qquad t \in [0,1], \qquad (26)$$

where V_G is the maximum gust intensity and the chosen "1+cos" gust profile reproduces an initial sudden perturbation of the flow which then fades out slowly.

Before the high- and low-fidelity gust response of the Typical Section were calculated, a low-fidelity aeroelastic stability analysis was carried out in order to define the safe aeroelastic flight envelope of the aircraft, by following the procedure presented in Appendix B and considering the aircraft to fly at sea level with a rigid angle of attack α_r =2deg; the reference wind speed V_∞ =15m/s was then suitably chosen, along with the gust intensity V_G =1.5m/s for a light gust and V_G =5m/s for a heavy gust. The "global" approach for calculating the additional aerodynamic load due to the gust has been employed alongside Theodorsen's theory, whereas the "local" approach is employed alongside Wagner's theory.

By combining the two airfoil shapes "A*i*" with the two couples of springs "S*j*" proposed in Table 1, four Typical Section configurations "A*i*-S*j*" are obtained as shown in Table 2 and their static and dynamic aeroelastic response investigated.

	S1	S2
A1	A1-S1	A1-S2
A2	A2-S1	A2-S2

Table 2: Typical Section configurations.

3.1 Static Response

Both low- and high-fidelity static aeroelastic responses of the Typical Section are presented in Table 3, for all its configurations.

	A1-S1	A2-S1	A1-S2	A2-S2
$\bar{h}_{LF}$	5.8mm	3.4mm	8.9mm	5.5mm
$\bar{h}_{HF}$	4.3mm	2.8mm	6.7mm	4.5mm
$\bar{\vartheta}_{LF}$	-0.216deg	-0.043deg	-0.529deg	-0.106deg
$\bar{\vartheta}_{HF}$	-0.176deg	-0.037deg	-0.404deg	-0.088deg

Table 3: Typical Section static response.

The low-fidelity results agree quite well with the high-fidelity ones, especially when the airfoil "A2" (which presents the lowest camber) is considered, since the springs displacements are actually small and the steady flow attached: the boundary layer is very thin and a steady potential-based theory is very efficient for estimating the airfoil's static aerodynamic load and predicts the static aeroelastic behavior of the Typical Section reliably enough at very low computational cost. Figure 4 shows the velocity vectors and streamlines of the aerodynamic flow around the two Karman-Trefftz airfoils as calculated by employing complex potential conformal theory.
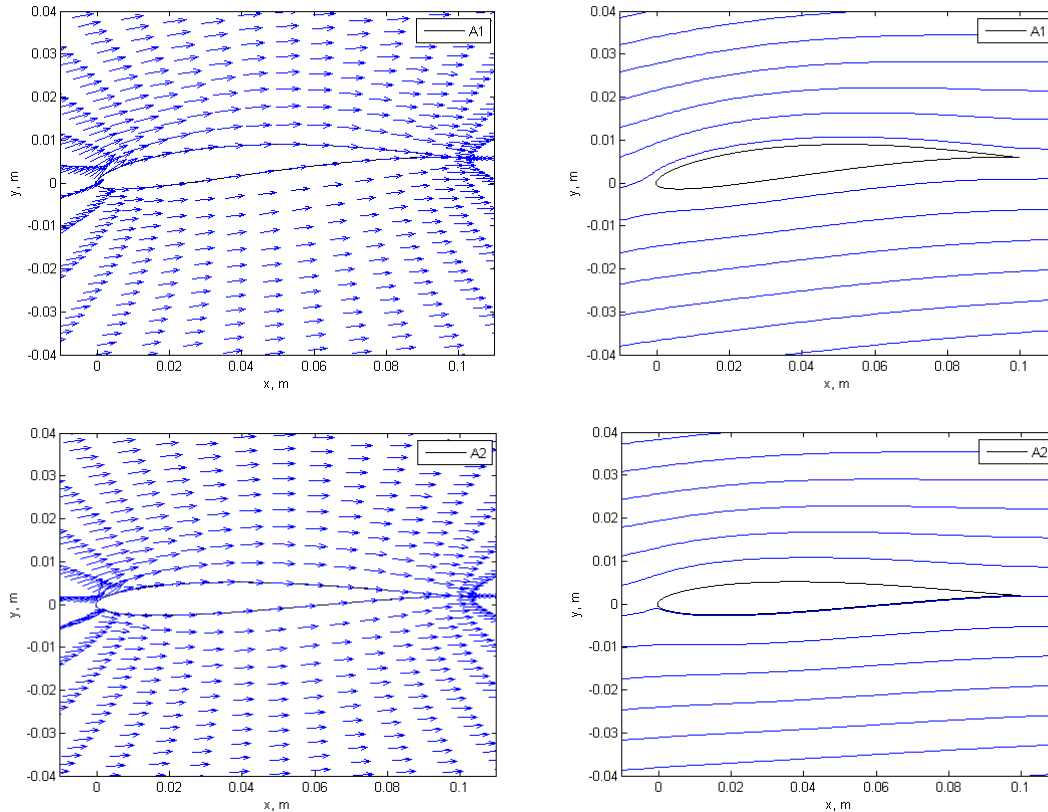

Figure 4: Velocity vectors and streamlines around the Karman-Trefftz airfoils.

3.2   Gust Response

In the case of a light gust, the aeroelastic dynamic response of the Typical Section is shown in Figure 5 for the two extreme configurations "A2-S1" and "A1-S2", which are characterized by the lowest airfoil camber with the largest spar width and the highest airfoil camber with the smallest spar width, respectively. Still, the low-fidelity results agree well with the high-fidelity ones, especially when the spar width "S1" (which leads

to the highest springs stiffness) is considered, since the springs displacements are actually small and the unsteady flow is attached: the boundary layer is thin (see Figure 6) and an unsteady potential-based theory is very efficient for estimating the purely dynamic aerodynamic load of the airfoil and predicts the dynamic aeroelastic behavior of the Typical Section reliably enough at very low computational cost.
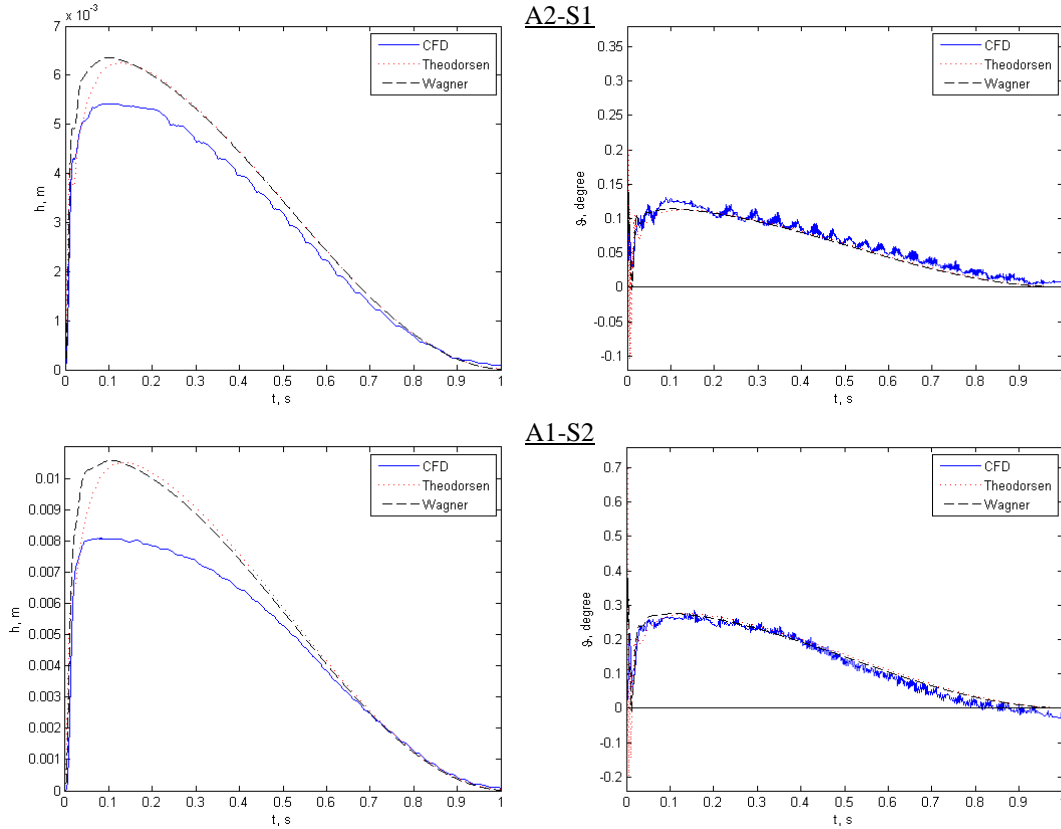

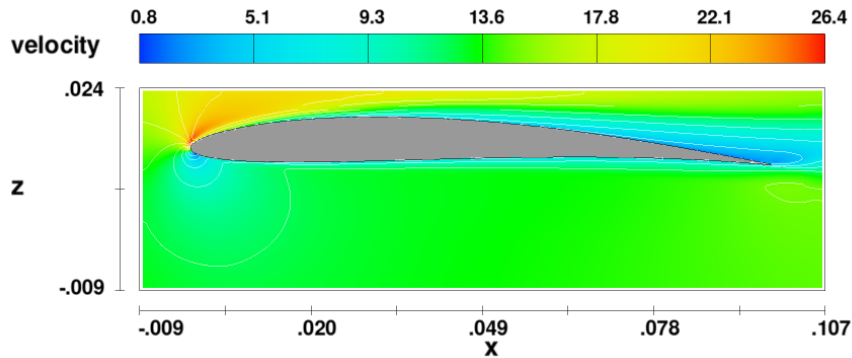Figure 5: Typical Section dynamic response to a light gust: vertical and torsional spring displacement.

Figure 6: Velocity magnitude contours for the Typical Section "A1-S2" dynamic response to a light gust.

In particular, agreement between the low- and high-fidelity results is generally better for the torsional spring displacement than for vertical spring displacement. However, during the initial transient of the gust response the opposite is true since the low-fidelity displacement of the torsional spring presents quite a high initial peak which is followed by very fast oscillations, especially in the case of the Theodorsen theory with the "global" gust approach. In fact, the presence of the initial peak in the low-fidelity results is due to the fact that the gust profile is initially described by a perfect step which is not

maintained in the CFD simulations, the gust profile of which is initially described by a very steep ramp instead. Moreover, the "global" gust approach employed along with Theodorsen theory provides the aerodynamic flow with additional apparent inertia, due to the variation in time of the vertical component of the free-stream velocity: this is not realistic in fact, since in a real situation the profile of a vertical gust is "frozen" in space (i.e., each point of the gust profile has a constant vertical speed) and the airfoil simply passes through it. No separation of the boundary layer being observed (see Figure 6), the small and very fast oscillations in the high-fidelity solutions represent the marginal effects of turbulence on the dynamic gust response of the Typical Section.

In order to overcome the issue of considering two slightly different gust profiles within the two models, the initial ramp of the gust profile provided by the high-fidelity model has been suitably approximated via an arctangent function and then employed within the low-fidelity model. Also, the contribution of the aerodynamic flow apparent inertia to the gust load of the "global" approach has been removed and the new results obtained are shown in Figure 7, focusing on the initial transient of the gust response.
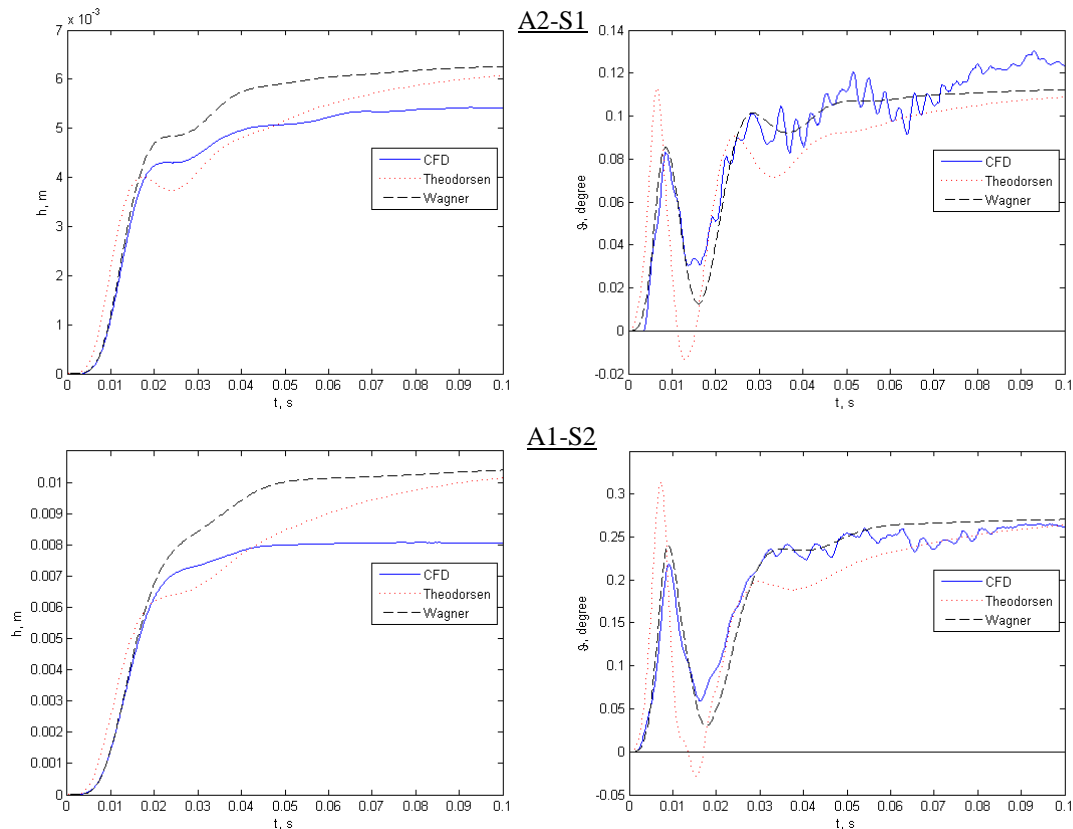

Figure 7: Typical Section dynamic response to a light gust: actual transient.

The agreement between low- and high-fidelity results is also very good during the initial transient of the gust response, especially for the torsional spring displacement. In particular, the results provided by Wagner's theory with the "local" gust approach are very accurate, whereas those provided by Theodorsen's theory with the "global" gust approach are slightly less accurate (since the airfoil's gradual penetration of the gust is not accounted for in the "global" approach) but computationally slightly cheaper (since there is no need for the additional differential equation for aerodynamic state describing the gust evolution in time). It's worth nothing that while Theodorsen's and Wagner's theories are formally equivalent, slightly different results can still be obtained due to the

accuracy of the particular approximations employed for both Theodorsen's and Wagner's functions in the range of the reduced frequencies and Strouhal number of the unsteady flow which characterises this study.

For the case of a heavy gust, the aeroelastic gust response of the Typical Section is shown in Figure 8 for the two extreme configurations "A2-S1" and "A1-S2", where the gust profile associated with the high-fidelity model has been suitably approximated and then employed within the low-fidelity model too.
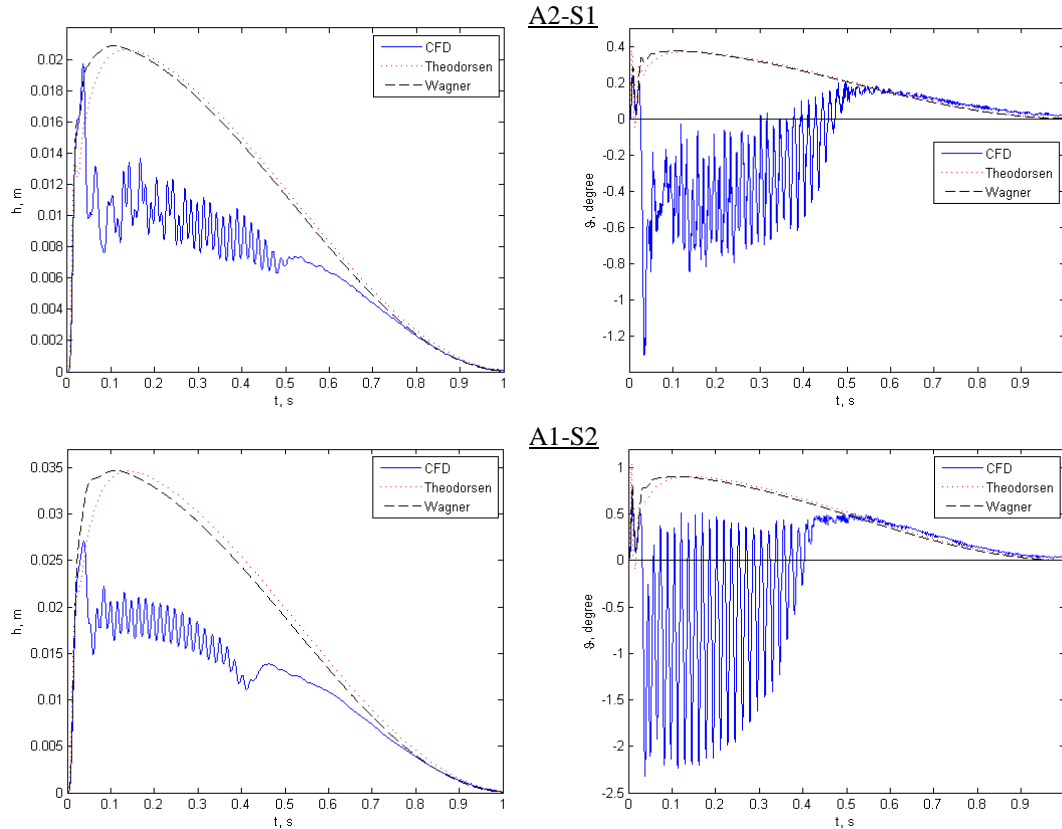

Figure 8: Typical Section dynamic response to a heavy gust: vertical and torsional spring displacement.

The low-fidelity results does not agree well with the high-fidelity ones, since the springs displacements are not small (especially that of the vertical spring) and the unsteady flow is separated: a linear potential-based theory is not effective for estimating the purely dynamic aerodynamic load of the airfoil and predict the nonlinear aeroelastic behavior of the Typical Section reliably enough in dynamic stall conditions[19]. Therefore, when a low-fidelity nonlinear stall model[20] is not employed, the low-fidelity response needs to be corrected according to the high-fidelity response, by employing a suitable tuning technique[21]. Nevertheless, it is possible to see how the results of the linear low-fidelity models agree well both at the very beginning and towards the end of the gust response: in the former case, the airfoil has not fully penetrated the gust yet and most of the flow around is still attached, whereas in latter case the vertical gust speed is gradually vanishing and the flow around the airfoil becomes attached again.

Figure 9 shows the evolution of a dynamic stall cycle for the Typical Section in terms of velocity field. It is possible to see the large periodic separation occurring at both the leading and the trailing edge (where a large eddy is shed in the airfoil wake), with detachment and reattachment of the aerodynamic flow around the airfoil; in

particular, it can be seen how the dynamics of the flow is driven by its vorticity rather than turbulence, due to the relatively low Reynolds number characterising this study.
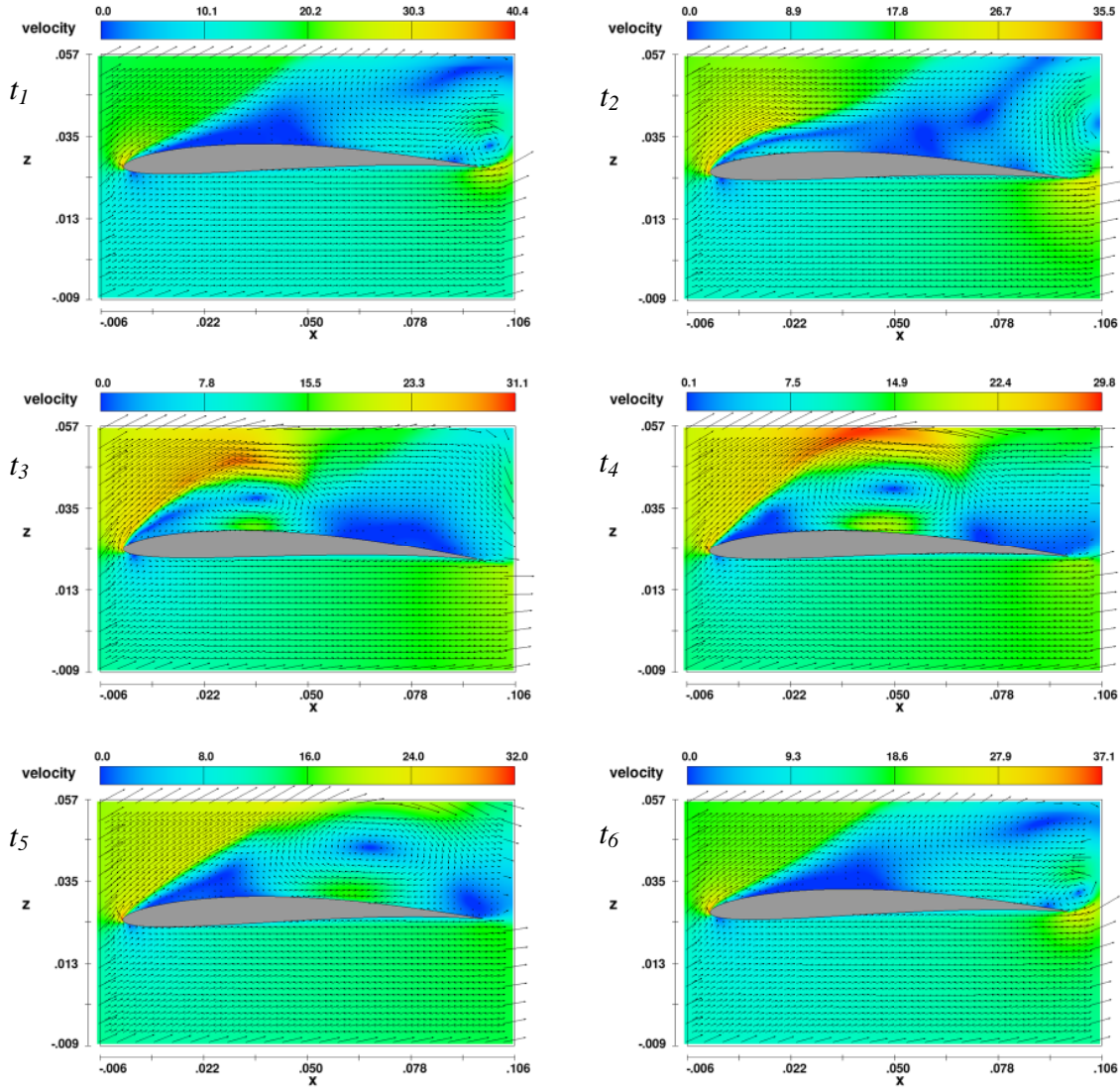

Figure 9: Typical Section "A1-S2" dynamic response to a heavy gust: velocity field around the airfoil.

4 CONCLUSIONS

The gust response of a Typical Section has been investigated in term of both a high-fidelity CFD solution and a low-fidelity analytical solution of the aerodynamic flow around it. Different airfoil shapes, Typical Section elastic properties, gust intensities and approaches ("local" and "global") have been investigated and the effects of the physical differences between the two modelling approaches have been identified in the case of both attached and separated flow. For attached flow, the low-fidelity aeroelastic gust response provided by Theodorsen's and Wagner's linear theories agrees well with the high-fidelity one provided by FLOW-3D; therefore, it can be concluded that both static and dynamic low-fidelity analytical aeroelastic models are suitable, fast and computationally cheap tools for use in the preliminary design of a flexible wing. In particular, the proposed state space form of the Wagner theory was found to be slightly more accurate than the proposed state space form of the Theodorsen theory, for the relatively high Strouhal number and reduced frequencies characterising this study, and

the Kussner approach demonstrated to be the most accurate for estimating the gust load in the low-fidelity model. For separated flow, the low-fidelity aeroelastic gust response does not exhibit the strong oscillations of the Typical Section in dynamic stall conditions, as correctly predicted by the high-fidelity model, and needs to be tuned by employing an appropriate technique; therefore, it can be concluded that both static and dynamic low-fidelity analytical aeroelastic solutions are not suitable for use in the advanced design of a flexible wing because of the high complexity of the physics involved in the very nonlinear fluid-structure interactions.

APPENDIX A: AEROELASTIC MATRICES AND AERODYNAMIC VECTOR

Static Response

$$[K] = \begin{bmatrix} k_h & -\frac{1}{2}\rho_\infty V_\infty^2 S C_{\overline{L}/\alpha} \\ 0 & k_\vartheta - \frac{1}{2}\rho_\infty V_\infty^2 Se C_{\overline{L}/\alpha} \end{bmatrix}, \qquad \{\overline{F}_r^a\} = \begin{Bmatrix} \frac{1}{2}\rho_\infty V_\infty^2 S C_{\overline{L}/\alpha}(\alpha_r - \alpha_0) \\ \frac{1}{2}\rho_\infty V_\infty^2 S\left(c C_{\overline{M}_{AC}} + e C_{\overline{L}/\alpha}(\alpha_r - \alpha_0)\right) \end{Bmatrix}. \quad (A1)$$

Dynamic Response: Theodorsen's Theory

$$[M^T] = \begin{bmatrix} m + \frac{\pi}{4}\rho_\infty Sc & -md - \frac{\pi}{4}\rho_\infty Sc\left(\frac{c}{4} - e\right) & 0 \\ -md - \frac{\pi}{4}\rho_\infty Sc\left(\frac{c}{4} - e\right) & \mu + md^2 + \frac{\pi}{4}\rho_\infty Sc\left[\frac{c^2}{32} + \left(\frac{c}{4} - e\right)^2\right] & 0 \\ \frac{0.468}{c} & -\frac{0.468}{c}\left(\frac{c}{2} - e\right) & 1 \end{bmatrix},$$

$$[C^T] = \begin{bmatrix} \frac{1}{4}\rho_\infty V_\infty S C_{\overline{L}/\alpha} & -\frac{1}{4}\rho_\infty V_\infty S\left[\left(\frac{c}{2} - e\right)C_{\overline{L}/\alpha} + c\pi\right] & 0 \\ \frac{1}{4}\rho_\infty V_\infty Se C_{\overline{L}/\alpha} & -\frac{1}{4}\rho_\infty V_\infty S\left(\frac{c}{2} - e\right)\left[e C_{\overline{L}/\alpha} - c\pi\right] & 0 \\ \frac{0.044}{V_\infty}\left(\frac{2V_\infty}{c}\right)^2 & -\left[0.234 + \frac{0.088}{c}\left(\frac{c}{2} - e\right)\right]\left(\frac{2V_\infty}{c}\right) & 0.552\left(\frac{2V_\infty}{c}\right) \end{bmatrix}, \quad (A2)$$

$$[K^T] = \begin{bmatrix} k_h & -\frac{1}{4}\rho_\infty V_\infty^2 S C_{\overline{L}/\alpha} & -\frac{1}{4}\rho_\infty V_\infty^2 S C_{\overline{L}/\alpha} \\ 0 & k_\vartheta - \frac{1}{4}\rho_\infty V_\infty^2 Se C_{\overline{L}/\alpha} & -\frac{1}{4}\rho_\infty V_\infty^2 Se C_{\overline{L}/\alpha} \\ 0 & -0.044\left(\frac{2V_\infty}{c}\right)^2 & 0.044\left(\frac{2V_\infty}{c}\right)^2 \end{bmatrix}.$$

Dynamic Response: Wagner's Theory

$$[M^W] = \begin{bmatrix} m + \frac{\pi}{4}\rho_\infty Sc & -md - \frac{\pi}{4}\rho_\infty Sc\left(\frac{c}{4} - e\right) & 0 \\ -md - \frac{\pi}{4}\rho_\infty Sc\left(\frac{c}{4} - e\right) & \mu + md^2 + \frac{\pi}{4}\rho_\infty Sc\left[\frac{c^2}{32} + \left(\frac{c}{4} - e\right)^2\right] & 0 \\ 0 & 0 & 1 \end{bmatrix}, \quad (A3)$$

$$[C^W] = \begin{bmatrix} \dfrac{1}{4}\rho_\infty V_\infty S C_{\overline{L}/\alpha} & -\dfrac{1}{4}\rho_\infty V_\infty S \left[\left(\dfrac{c}{2}-e\right)C_{\overline{L}/\alpha}+c\pi\right] & 0.054\rho_\infty V_\infty S C_{\overline{L}/\alpha}\left(\dfrac{2V_\infty}{c}\right) \\ \dfrac{1}{4}\rho_\infty V_\infty Se C_{\overline{L}/\alpha} & -\dfrac{1}{4}\rho_\infty V_\infty S\left(\dfrac{c}{2}-e\right)\left[eC_{\overline{L}/\alpha}-c\pi\right] & 0.054\rho_\infty V_\infty Se C_{\overline{L}/\alpha}\left(\dfrac{2V_\infty}{c}\right) \\ -1 & \left(\dfrac{c}{2}-e\right) & 0.3455\left(\dfrac{2V_\infty}{c}\right) \end{bmatrix},$$

$$[K^W] = \begin{bmatrix} k_h & -\dfrac{1}{4}\rho_\infty V_\infty^2 S C_{\overline{L}/\alpha} & 0.0034\rho_\infty V_\infty S C_{\overline{L}/\alpha}\left(\dfrac{2V_\infty}{c}\right)^2 \\ 0 & k_\vartheta -\dfrac{1}{4}\rho_\infty V_\infty^2 Se C_{\overline{L}/\alpha} & 0.0034\rho_\infty V_\infty Se C_{\overline{L}/\alpha}\left(\dfrac{2V_\infty}{c}\right)^2 \\ 0 & V_\infty & 0.136\left(\dfrac{2V_\infty}{c}\right)^2 \end{bmatrix}.$$

APPENDIX B: AEROELASTIC STABILITY ANALYSIS

Consider a generic linear aeroelastic system

$$[M]\{\ddot{x}\}+[C]\{\dot{x}\}+[K]\{x\}=\{F\}. \tag{B1}$$

The static aeroelastic divergence speed V_D is defined as the minimum speed V_∞ that makes the static response of the aeroelastic system singular and can be investigated globally as the minimum aircraft speed for which[22]

$$\det([K])=0; \tag{B2}$$

meaning that the elastic forces of the flexible structure are not able to balance the static aerodynamic forces acting over it and eventually guarantee a unique static equilibrium point anymore.

The dynamic aeroelastic divergence speed V_F (flutter speed) can be defined as the minimum speed V_∞ that leads the real part of at least one of the eigenvalues λ of the aeroelastic system being positive, hence making its dynamic response singular, and can be investigated globally as the minimum aircraft speed for which[23]

$$\det([M]\lambda^2+[C]\lambda+[K])=0; \tag{B3}$$

flutter being due to coupled self-sustained motion of at least two degrees of freedom of the aeroelastic system, one of which becomes unstable and extracts energy from the other/s (hence becoming more stable) involved in the coupling mechanism. A polynomial characteristic equation is obtained from the condition above and an even number of eigenvalues is calculated numerically for each aircraft speed within the target flight envelope. These eigenvalues are generally complex numbers $\lambda_i = \delta_i + i\omega_i$ that are aircraft speed dependent and can be either all real, or some real and some complex conjugates, or all complex conjugates: the real part δ_i relates directly to the damping of

the system, whereas the imaginary part ω_i relates directly to the frequencies f_i of the system as $\omega_i = 2\pi f_i$. For $V_\infty = 0$m/s the aeroelastic system is not aerodynamically damped by definition; therefore, the real parts of its eigenvalues are zero and its structural natural frequencies obtained[24].

AKNOWLEGDEMENTS

REFERENCES

[1] Livne, E., "The Future of Aircraft Aeroelasticity", *Journal of Aircraft*, Vol. 40, No. 6, 2003.

[2] Hodges, D.H., Pierce, G.A., *Introduction to Structural Dynamics and Aeroelasticity*, Cambridge University Press, 2002.

[3] Flow Science, *FLOW-3D v.9.4*, Flow Science Inc., 2009.

[4] Theodorsen, T., "General Theory of Aerodynamic Instability and the Mechanism of Flutter", NACA TR-496, 1935.

[5] Wagner, H., "Uber die Entstenhung des dynamischen Auftriebes von Tragflugeln", *Zeitschrift für Angewandte Mathematik und Mechanik*, Vol. 5, No 1, 1925.

[6] Quartapelle, L., *Numerical Solution of the Incompressible Navier-Stokes Equations*, Birkhäuser, 1993.

[7] Chung, T.J., *Computational Fluid Dynamics*, Cambridge University Press, 2002.

[8] Orszag, S.A., Yakhot, V., Flannery, W.S., "Renormalization Group Modeling and Turbulence Simulations", In: *Near-Wall Turbulence Flows*, Elsevier, 1993.

[9] Glauert, H., *The Elements of Aerofoil and Airscrew Theory*, Cambridge University Press, Cambridge, 1947.

[10] Garrick, I.E., "Propulsion of a Flapping and Oscillating Airfoil", NACA TR-567, 1936.

[11] Katz, J., Plotkin, A., *Low Speed Aerodynamics*, Cambridge University Press, 2001.

[12] Venkatesan, C., Friedmann, P.P., "New Approach to Finite-State Modelling of Unsteady Aerodynamics", *AIAA Journal*, Vol. 24, No. 12, 1986.

[13] Jones, R.T., "The Unsteady Lift of a Wing with Finite Aspect Ratio", NACA TR-681, 1940.

[14] Zaide, A., Raveh, D., "Numerical Simulation and Reduced-Order Modeling of Airfoil Gust Response", *AIAA Journal*, Vol. 44, No. 8, 2006.

[15] Kussner, H.G., "Zusammenfassender Beritch uber den instationaren Auftrieb von Flugeln", *Luftfahrtforsch*, Vol. 13, No. 2, 1936.

[16] Karamcheti, K., *Principles of Ideal-Fluid Aerodynamics*, Krieger, 1980.

[17] Bisplinghoff, R.L., Ashley, H., Halfman, R.L., *Aeroelasticity*, Addison-Wesley, 1955.

[18] Young, W.C., Budynas, R.G., *Roark's Formulas for Stress and Strain*, McGraw-Hill Professional, 2001.

[19] Dowell, E.H., et al., *A Modern Course in Aeroelasticity*, Kluwer, 2004.

[20] Meyer, M., Matthies, H.G., "State-Space Representation of Instationary Two-Dimensional Airfoil Aerodynamics", *Journal of Wind Engineering and Industrial Aerodynamics*, Vol. 92, No. 3-4, 2004.

[21] Berci, M., Toropov, V.V., Hewson, R.W., Gaskell, P.H., "Modelling based on High and Low Fidelity Models Interaction for UAV Gust Performance Optimization", AIAA-2009-2215, 2009.

[22] Wright, J.R., Cooper, J.E., *Introduction to Aircraft Aeroelasticity and Loads*, AIAA Education Series, 2007.

[23] Bielawa, R.L., *Rotary Wing Structural Dynamics and Aeroelasticity*, AIAA Education Series, 2006.

[24] Fung, Y.C., *An Introduction to the Theory of Aeroelasticity*, Dover, 1993.